Conference Paper

Flow visualization of projectile-sabot separation in a pulsed wind tunnel in comparison with numerical simulations

Author(s):
Reck, Bernhard; Hruschka, R.; Sauerwein, B.

Publication Date:
2018-10-05

Permanent Link:

https://doi.org/10.3929/ethz-b-000279198 →

FLOW VISUALIZATION OF PROJECTILE-SABOT SEPARATION IN A PULSED WIND TUNNEL IN COMPARISON WITH NUMERICAL SIMULATIONS

B. Reck[1,c], R. Hruschka[2], B. Sauerwein[2]

[1]French-German Research Institute of Saint-Louis (ISL), ERG Group, 68301 Saint-Louis, France
[2]French-German Research Institute of Saint-Louis (ISL), AMS Group

[c]Corresponding author: Tel.: +33 389 69 5178; Fax: +33 389 69 5193; Email: bernhard.reck@isl.eu

KEYWORDS:
Main subjects: relative motion of bodies in a high speed flow region, body trajectories
Fluid: high speed flows with shocks
Visualization method(s): differential interferometry, numerical density contour plots
Other keywords: numerical model, hydrocode

ABSTRACT: *The transient separation process of a sabot from a projectile simulant is experimentally investigated in a short-duration wind tunnel. Using a generic model of simple geometry in combination with well-known flow conditions in the tunnel allows creating an accurate set of measurement data. These data include differential interferometry (schlieren-like) flow visualization, sabot trajectories and transient pressure signals at a fixed center sting, simulating the projectile behavior after exiting the gun tube. This well defined data set was used to evaluate and to validate numerical simulation models. In our case we chose the AUTODYN-hydrocode which describes the gaseous fluid by means of an Euler method, and the sting and the sabot components are represented by Lagrangian parts which are each coupled with the Eulerian gas part. Three different cases were chosen for the comparison between the shock tunnel experiments and the numerical simulation: a sabot consisting of two components that are symmetrically placed around the sting, a single sabot component placed on the sting, and a single sabot component put into the flow without the sting. By comparing the differential interferometry images with the numerical contour density plots, and further comparing the experimental and numerical sabot trajectories, we found an very good, despite the fact that the Euler method does not account for friction in the gas flow.*

1 Introduction

High velocities of projectile are usually achieved in powder guns by using sub-caliber ammunition, i.e. the projectile caliber is smaller than the gun caliber. The projectile is centered inside the gun tube by a sabot, which transmits the propulsive loads during acceleration and ensures gas sealing. The sabot components need to be discarded after muzzle exit. The challenge is to minimize the disturbances to the projectile flight trajectory. Typical issues are, e.g. sabot-projectile contact, and aerodynamic interference caused by flow asymmetry which may result in an asymmetric sabot separation process [1].

Numerical modeling is a convenient method to analyze and to understand the different stages of this transient process, and in particular, to perform optimization tasks. However, depending on the capabilities of the computation code, and depending on the skills and experience of the expert, there might be a lack of confidence in the results, in particular if an accurate comparison with experiments is not available. In order to make this comparison, the sabot separation process was simulated experimentally in a shock tunnel under thoroughly defined conditions using a simplified model. Differential interferometry measurement technique provided schlieren-like images, and pressure data

were gathered under reproducible conditions. These data can be used to evaluate the numerical simulation results.

2 Shock Tunnel Experiments

2.1 Test Setup

The test series were performed in the ISL shock tunnel [2]. The schematic view of the test setup inside the tunnel is shown in Fig. 1, together with the dimensions of the sabot-sting combination. . The projectile is represented by a steel center sting which is anchored as a cantilever. The sting nose is conical with an opening angle of 30°. In the full sabot test case, two Nylon segments are loosely attached to the sting, each covering 180° of the cylindrical surface (Fig. 2, case A, left). The design was adapted from Schmidt et al. [3], except that two sabot segments instead of three are spanning 120° in ref. [3] as well as a different model scale. The diameter d is here equal to 10mm. Fig. 2 shows two additional configurations which were investigated within this work: a single sabot component placed on the upper side of the sting (case B), and eventually the upper sabot component without sting or "sabot-only" case (C). All sabot components have identical geometry, with a chamfered leading edge of 40° angle.

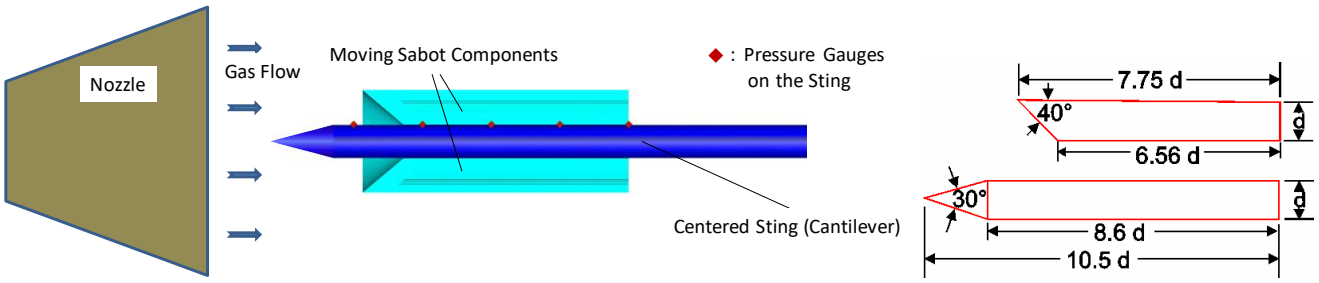

Fig. 1. Schematic view of the shock tunnel setup (left) and dimensions of the model (right).

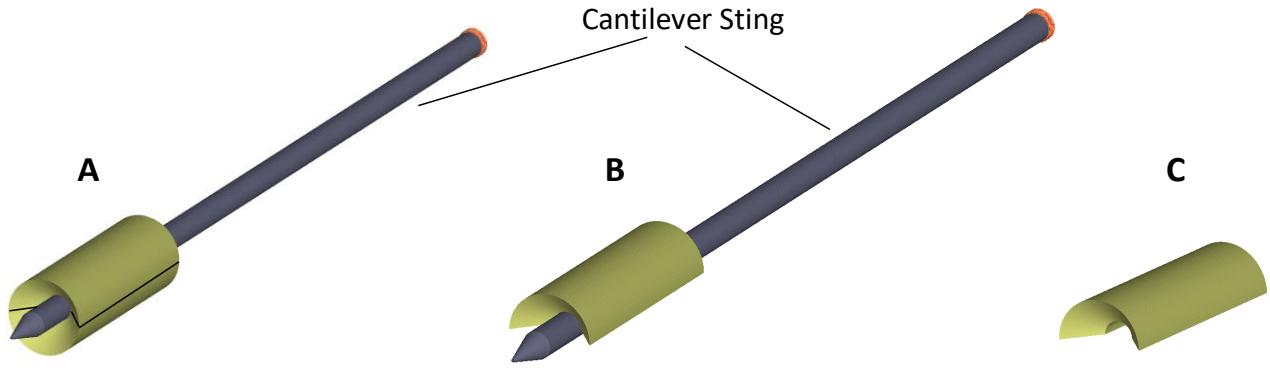

Fig. 2. Shock tunnel test cases, left to right: A, two-component full sabot symmetrically arranged on the sting, B, single sabot component on the sting, and C, single sabot component without sting ("sabot only" configuration)

For the visualization of the gas flow, differential (or schlieren-like) interferometry is applied. The images are captured at about 4×10^4 frames per second. Moreover, five pressure gauges are flush-

mounted on the upper sting surface at distances of 20 mm in between (Fig. 1), in order to collect data for a detailed analysis of the flow region close to the sabot-sting interface.

2.2 Flow Conditions

All tests were conducted under identical flow conditions, i.e. nitrogen (R=296.8 J/kg/K) enters the test section at Mach 4.5, which is initially evacuated. Successively, quasi-steady gas flow can be maintained at a static temperature of 245 K and 0.13 bar pressure for approximately 4 milliseconds. That duration has proved to be sufficient for studying the principal stages of the sabot separation process.

3 Numerical Simulation

The simulation of shock interaction with structures at very short time frames is frequently handled by hydrocodes, numerical simulation codes that were originally developed for studying transient mechanical phenomena in the range between several microseconds and hundreds of milliseconds. A broad variety of ballistic phenomena can be addressed, e.g. projectile-target interaction, detonation, explosions in air. An example of the successful comparison of hydrocode results with experimental values is described in [4], inspiring the present work.

The computation in the context of this work was performed with Ansys Autodyn [5]. It provides an Euler solver [6] for modeling the gas part and a Lagrange solver for modeling the structural parts, i.e. solids and shells. All parts can interfere with each other by coupling algorithms. In contrast to advanced CFD-codes based on Navier-Stokes equations, the Euler solver cannot take into account viscous phenomena in the fluid part. Its limitation to inviscid flow can be generally considered as a drawback, but within the context of short duration phenomena it is interesting to see at the end of this study, if viscous effects actually have a significant effect on the momentum transfer from the gas fluid to the sabot. On the other hand, hydrocodes have undeniable advantages since contact between the structural parts is included. Due to contact and impact loading and due to aerodynamic loading, the structural parts can undergo large deformations, damage and fracture, which in turn, affects the conditions of the flow around these parts.

3.1 Numerical mesh

The Euler mesh and the meshes for the sting and sabot components are shown in Fig. 3 and Fig. 4. Lagrange solid meshes are used for the sabot parts. The sting is modeled by Lagrange shell elements in the full sabot case (Fig. 4, A) to reduce the computational costs. This model has two symmetry planes intersecting on the sting axis and therefore, only a quarter of the whole problem needs to be modeled. The one-sabot-component configuration is built as half model (Fig. 4 B). In contrast to case (A), the sting center axis is not a symmetry axis. The flow impulse now sets the solid sting in vertical motion. In order to correctly compute the body inertia, the sting needs a solid-(volume)-mesh. The “sabot-only” case is shown in Fig. 4 C. As for case (B), one half of the problem is modeled, but the whole sabot component is presented in Fig. 4 for clarity.

Unlike advanced CFD codes, Autodyn does not provide adaptive meshing of the fluid part. The initially defined finite-volume Euler mesh remains constant with time. Small gaps between two structural parts, which here are the sting and the sabot, need to be modeled by even smaller mesh elements from the start, in order to simulate fluid penetration. However, the Autodyn hydrocode needs to keep the balance with computation time, depending on the hardware resources and parallel computing capabilities. Therefore, in contrast to the pressure gauges of the experimental setup (Fig. 1,

red diamond symbols), the numerical pressure gauges, located in the tiny gap between sting and sabot, are not able to show pressure values in the early stage before the sabot component starts to separate from the sting.

3.2 Model setup

An ideal gas equation-of-state is used for the nitrogen gas in the Euler part. The initial condition in the flow part was set to nitrogen at 20 Pa pressure and zero velocity to simulate a low pressure environment also present before the wind tunnel experiment. The gas starts entering the Euler part on the in-flow boundary at time t = 0 ms at constant velocity and 13 kPa constant pressure. This is a simplifying assumption for computational reasons and is different from the experimental setup. In the latter case, the time which the flow takes to travel through the nozzle and to establish comparable flow conditions is about 0.5 milliseconds. The numerical flow-out condition is defined on the opposite face, and partially on the lateral faces (see Fig. 3) in order to avoid shock reflections from the mesh boundaries.

The material for the sting is steel (density 7.83 g/cm³) with standard elastic behavior (Young's modulus 210 GPa, Poisson's ratio 0.3). Nylon 6 (density 0.98 g/cm³) was chosen for the sabot components. This material is light-weight and therefore ensures the separation process within the available time span. Elastic deformation is described by 0.85 GPa Young's modulus and 0.44 Poisson's ratio. A yield strength criterion was added showing that, for all computations, the nylon material never entered the plastic strain region.

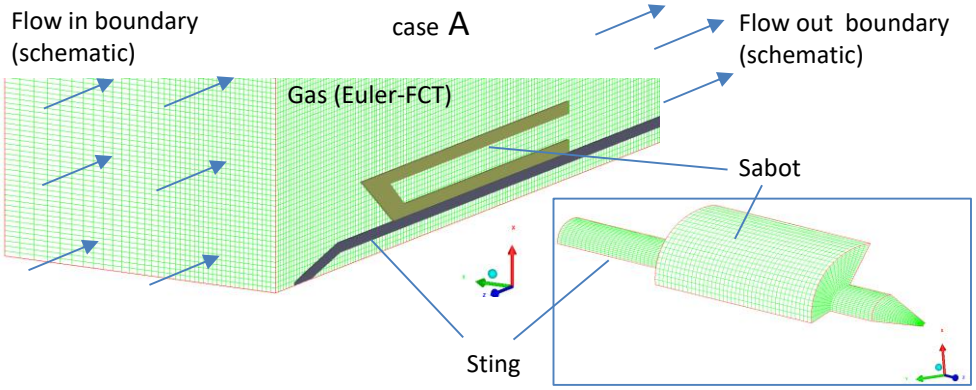

Fig. 3. Numerical Euler mesh for the gas part and Lagrange meshes for sabot and sting, case A, two-component full sabot and sting, quarter-model,.

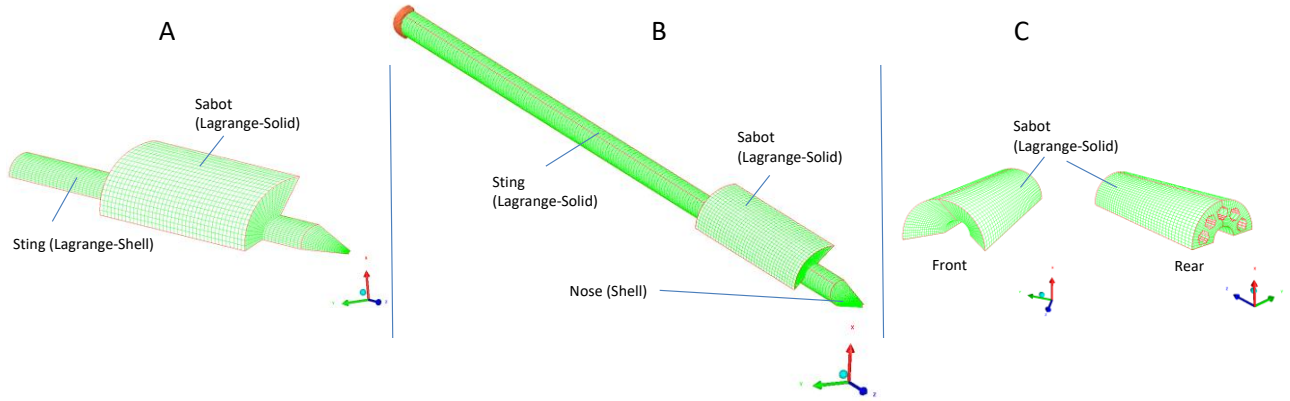

Fig. 4. Numerical meshes, left to right: A, quarter-model for the two-component full sabot and sting, B, half model for the single-sabot component with sting and C, "sabot-only" configuration

4 Comparison between experiment and numerical simulation

4.1 Differential interferometry images versus numerical density-contour plots

For a suitable comparison of the differential interferometry images with the numerical results, we chose the density-contour plot option from the built-in Autodyn post-processing environment. Fig. 5 shows a direct side-view to the symmetry plane of the different models. The corresponding center section of the sabot is visible, not its rectangular projection, as seen on the interferometry images. Therefore a red rectangle was added for better comparison.

All numerical images in Fig. 5 were plotted at time t=2 ms after in-flow start through the mesh boundary and compared with the schlieren images of the corresponding spatial sabot position. This choice is not related to a particular phenomenon, but rather to show the good agreement between experiment and computations when the sabot is going to separate and the flow field looks relatively complex. The front shocks of the sting and the sabot are well represented by the numerical model. However, we have to keep in mind that the friction-related flow phenomena cannot be taken into account by the Euler method. Those areas can be observed, in particular, on the schlieren image (top right, A) close to the sting surface behind sting nose shock. The center images (case B) in Fig. 5 show the asymmetric case of a single sabot component separating from the sting. Five numerical gauge points fixed (red diamonds, left) in the Euler gas space were originally located on the sting surface. Referring to these positions, we observe that the sting in the numerical model has moved downward due to the high pressure region on its upper surface when the sabot component separates (see also §4.4, vertical sting motion). The “sabot-only” numerical density plot (case C, Fig. 5. bottom) shows, like in the previous cases A and B, an excellent agreement with the corresponding schlieren image.

4.2 Trajectory and angle of attack of the sabot components

For each of the three different test cases A, B and C, the quantitative motion of the sabot components is plotted in Fig. 6. We chose the trajectories of the sabot center of gravity in the horizontal and vertical direction as a function of time, and further, the time-dependent angle of attack. The experimental data of case A, i.e. full sabot with sting, are presented by average values of 4 tests having very little dispersion. For each of the other two cases (B and C), the numerical results are compared with two distinct experimental data sets tagged with the corresponding test number.

The experimental sabot motion is generally faster than the simulated motion after three to four milliseconds separation time for all cases. Case A and case B need to be briefly discussed in detail.

Case A, two-component sabot configuration: The numerical displacement curves have an initially steeper slope than the corresponding experimental values. This is probably due to the difference of the initial in-flow conditions. The numerical in-flow starts instantaneously and can be characterized by a pressure jump. It takes about 0.2 milliseconds to arrive at the sabot front side, while the experimental flow is characterized by a ramp rising from almost zero pressure to 0.13 bar within about 0.5 milliseconds. The pressure jump of the numerical model generates higher initial pressure which, in combination with the partially confined space in front of the chamfered sabot, contributes to an additional impulse load. At a later separation stage, the experimental sabot "overtakes" the numerical sabot.

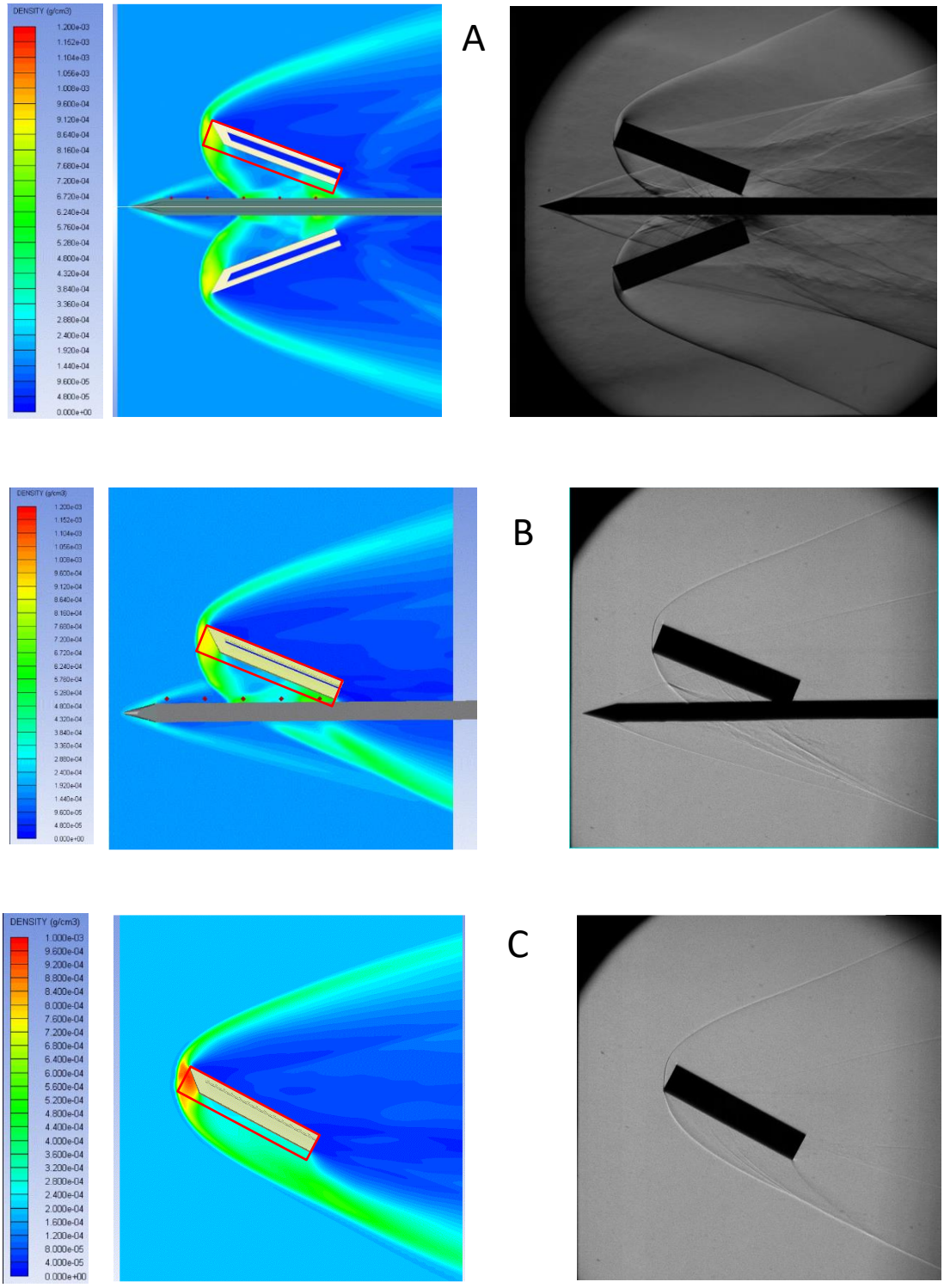

Fig. 5. Density-contour plot of the numerical models at t= 2ms (left) vs. corresponding schlieren image (right). Top: Two-component full sabot with sting, Center: Single-sabot component and sting, Bottom: "Sabot-only"

Case B, single sabot component with sting: The horizontal sabot displacement (left) is similar to case A. The computed horizontal displacement curve is initially rising faster than the experimental curve, but to a smaller extend compared the full sabot case A. The confinement effect between single sting and sabot component is less pronounced here.
In Fig. 7 the center-of-gravity-trajectories of the sabot components for each of the investigated cases are presented. The numerical results fit very well with the test data, except for the "sabot-only" configuration, case C. The experiments indicate an approximately 10% higher vertical lift at t=4 ms compared to the numerical model, in which the difference seems to appear at the initial stage. Besides the fact that the Euler method does not account for friction in the flow, a further cause might be the interference between the sabot and its light-weight supporting structure in the test tunnel. This possibility is currently not considered in the numerical model and will be investigated in the future.
The comparison shows that the numerical results are in very good agreement with the test data, which was not expected prior to this study. Nevertheless as a general tendency concerning the numerical simulation, we observe a slower sabot motion compared to the measured values. On the one hand, this can be attributed to the Eulerian description of the flow in the numerical models which does not consider viscous effects. Therefore friction cannot contribute to the momentum increase of the sabot components during the separation process. On the other hand, the slight mismatch between numerical and experimental results could be related to the way, the Eulerian fluid and the Lagrangian structural parts interact with each other in Autodyn. The "strong coupling"-option was used with the default settings. One parameter is the "cover fraction limit" set to 0.5 by default. It defines the threshold at which a partially covered cell is blended to a neighbor cell [7]. Investigations showed that modifications of this parameter did not change the result significantly.

4.3 Pressure on the sting surface

The pressure measurement on the sting and the comparison with numerical simulation is described for the two-component full sabot configuration (case A). The measured pressure of the five gauges is plotted in Fig. 8, which represents the values of one specific test. It has to be mentioned that the shock tunnel tests provide highly reproducible data. The significant oscillation is due to the transient bow shock which is a typical phenomenon of spiked bodies in supersonic flow [8]. For the sake of clarity the gauges #3 and #5 are depicted to compare their pressure curves with the corresponding calculated values from numerical simulation. In addition, the images next to the plots (Fig. 9, right) show the flow field at the time when the sabot front shock touches gauge #3 at t=2.02 ms and at a later stage, gauge #5 at t=2.56 ms.
Gauge #3, Fig. 9 top: The numerical pressure between 0.5 ms and 1 ms is greater than the experimental value, indicating that the initial in-flow is modeled as pressure jump in contrast to the experimental in-flow, characterized by a pressure ramp (see previous paragraph §4.2). Prior to t= 0.5 ms the numerical gauge does not see any pressure, because the gap between sting and sabot is too small for flow penetration (see also §3.1). Later at t=2.02 ms, a distinct pressure decay is observed for both, the experimental and the numerical curves, when the sabot front shock passes over the gauge.

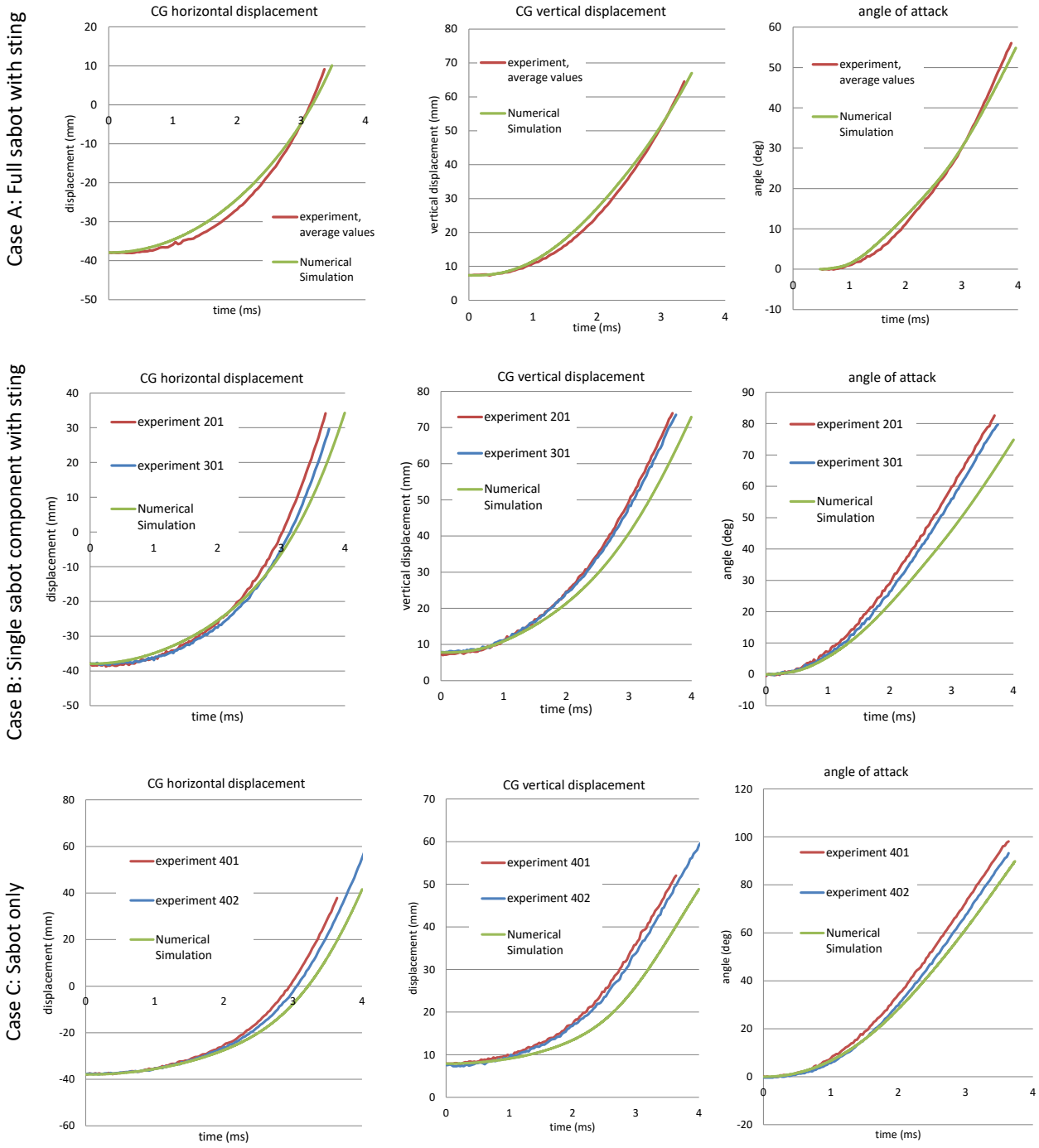

Fig. 6. Sabot center-of-gravity (CG) displacement and angle of attack. Top: A, two-component sabot configuration, center: B, single sabot component with sting, bottom: C, "sabot only" configuration

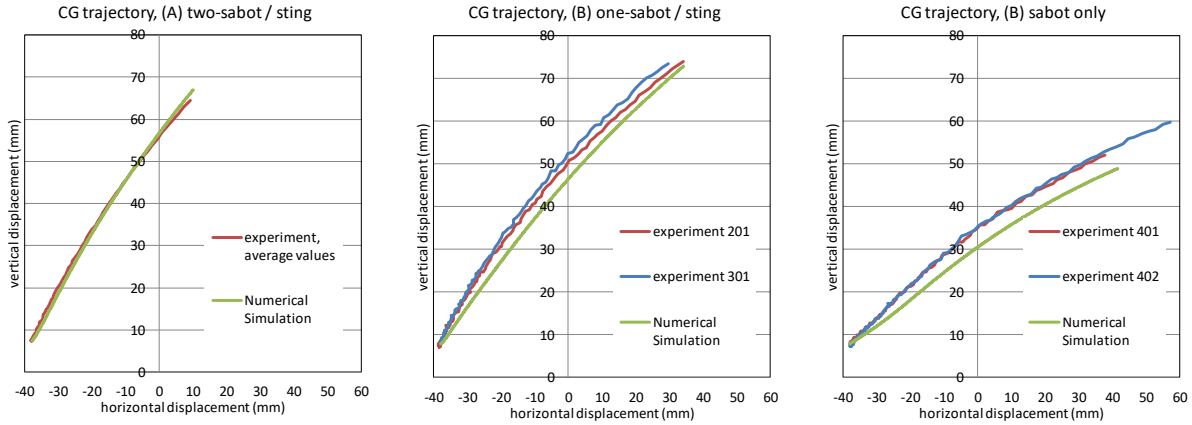

Fig. 7. Sabot center-of-gravity (CG) displacement and angle of attack. Top: A, two-component sabot configuration, center: B, single sabot component with sting, bottom: C, "sabot only" configuration

Gauge #5, Fig. 9 bottom: The measured pressure curve shows strong oscillations in contrast to the numerical values. This can be assigned to friction along the sting surface and therefore is not visible in the numerical Euler flow field. Both, numerical and experimental curves decay significantly after the sabot front shock has moved over the gauge at about t=2.5 ms. Gauge 5 is located at the initial position of the sabot base. The numerical gauge sees the flow arriving from behind, i.e. the pressure rises up to 0.13 bar until t=0.6 ms. Then the sabot starts moving horizontally, covering the gauge which in turn is isolated from the flow and cannot not indicate any pressure. The pressure signal appears again at about t=1 ms when the sabot starts to separate and the gap between sting and sabot increases.

The comparison of the pressure data, obtained from the experiment and from numerical simulation, highlights some principal differences. This is in particular true for the gap between sting and sabot, which is initially small, and can be a challenge for numerical codes. If adaptive meshing is not an option, like in the current study, differences between numerical simulation and experimental work cannot be avoided inside gaps which are smaller than the local cell size of the fluid mesh.

The modeling of the pressure gauges on the sting of the single-component sabot (case B) was not done within this work. This task is rather demanding, because the numerical gauges need to be placed at fixed positions in the Euler space, while the pressure gauges in the experiment are mounted on the sting. Since the sting is moving vertically in case B, the numerical and experimental positions are drifting apart. A solution for future investigations might be the use of an array of gauges that are set in the Euler space along the travel path of each experimental gauge.

4.4 Vertical sting motion

The experimental setup consists of an elongated cantilever sting which, for the full-sabot two-component configuration (case A), remains fixed in space due to the symmetries of geometry and aerodynamic loading. However, the single sabot component configuration is asymmetric (case B), and therefore the sting is prone to bending. This case could be used as an additional example to verify the Euler-Lagrange-interaction capabilities of the numerical model. Due to the constraints at the attachment, horizontal motion of the sting can be neglected. Its behavior is that of an elastic cantilever beam, and thus is bending downward, while the sabot component separates toward the opposite side.

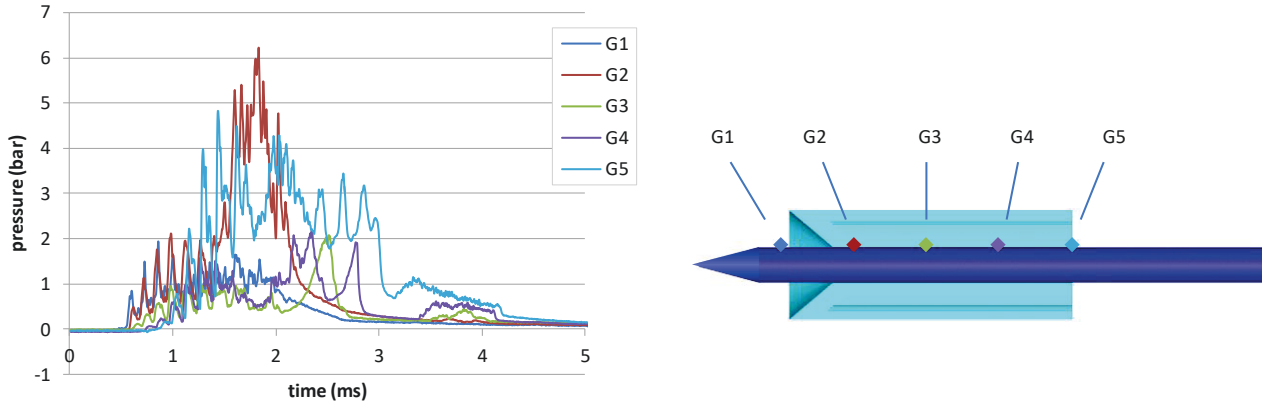

Fig. 8. Measured gauge pressures on the sting surface°

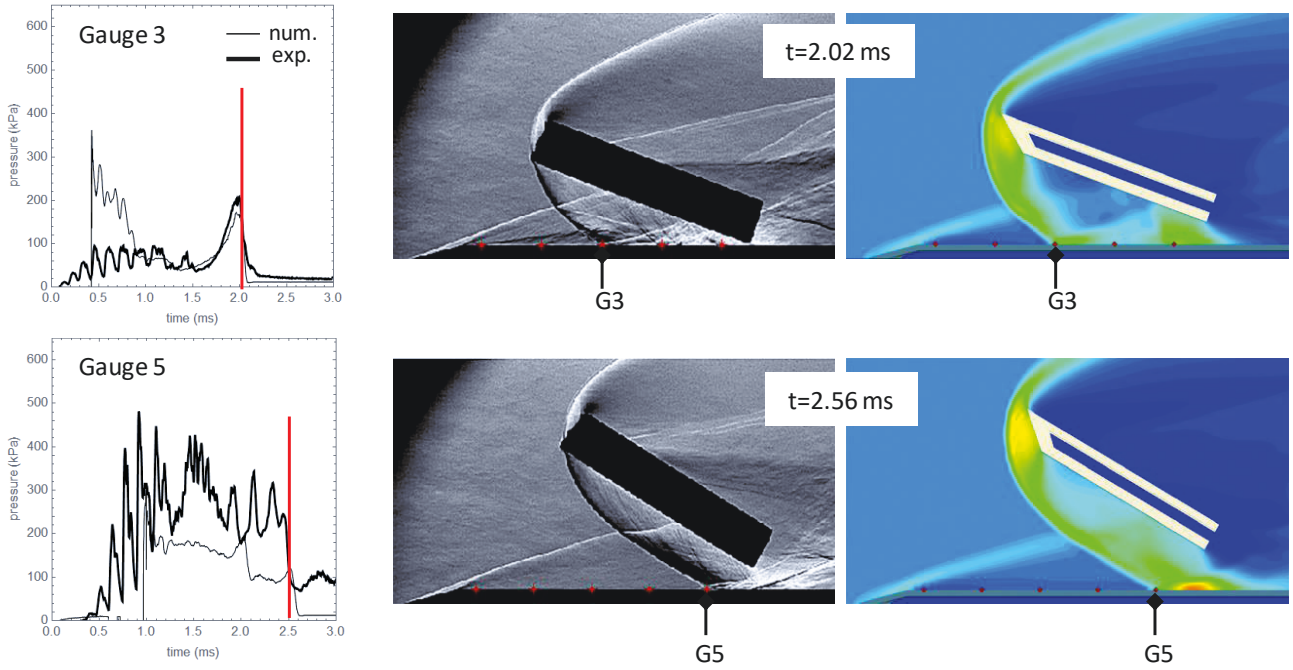

Fig. 9. Pressure values of gauge # 3 and #5 and flow fields when sabot front shock touches gauges

The calculated time-dependent vertical sting displacement (red line), of a point located close to the sting nose, is plotted in Fig. 10 (left). The three experimental values are corresponding to 60°, 75° and 90° angle of attack, respectively. As stated in §4.2 and visible on Fig. 6, the calculated motion is slightly delayed compared to the experiment. For identical angles of attack, the measured sting displacement almost matches with the numerical data, as indicated by the angle-of-attack values "aa = 90°".

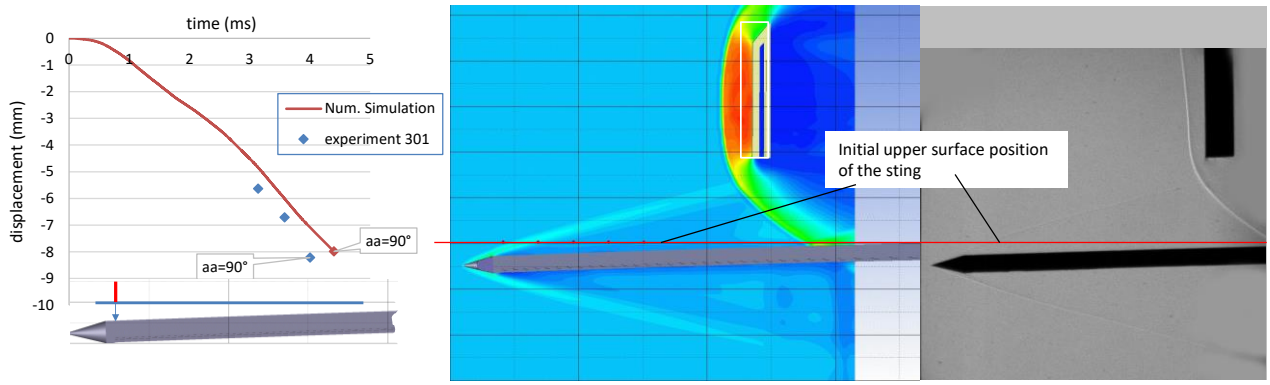

Fig. 10. Vertical displacement of the sting, case B (single sabot component). Density contour plot (center) and schlieren image (right) at sabot angle of attack (aa) = 90°

5 Conclusions

Sabot separation experiments were performed in the ISL-shock-tunnel. The projectile is simulated by a fixed sting, instrumented with pressure gauges. Three different cases were investigated: The symmetrical full-sabot configuration, consisting of a simplified two-component sabot, a one-sabot-component configuration using a single sabot component on the sting, and the latter configuration without sting, also named “sabot-only” case.

The three cases were modeled numerically using a hydrocode. The flow simulation is based on the Euler method, while the sting and the sabot components were modeled as Lagrangian parts, interacting with each other and with the Euler fluid. Viscous effects in the fluid part are therefore not considered by the numerical model.

The trajectories and the angle of attack of the sabot components were calculated and compared with the experimental results. The time-dependent displacement plots show a slightly delayed motion of the numerical sabots. This behavior is most likely due to the fact that the Euler method is limited to inviscid flow. Despite that "simplification", a surprisingly good agreement between numerical results and the experimental data can be observed. The spatial trajectories evaluated from the experiments are very close to the data calculated from numerical simulation, except the vertical sabot displacement of the “sabot-only” case. During the initial stage, the numerical sabot motion is slower than the measured motion. A possible interference between the sabot and its light-weight supporting structure in the test tunnel is under investigation.

Additionally for the full-sabot configuration, the experimental values of the flow pressure on the sting surface were compared with the corresponding numerical values. Bow shock oscillation appears, which is typical for spiked bodies. Basic phenomena like the passage of the sabot front shock during separation can be observed on both, the experimental and the numerical pressure curves. However some significant pressure variations are friction related and thus cannot be shown by means of the Euler flow simulation.

Euler-Lagrange hydrocode models are able to compute sabot trajectories in a reliable way within the time span of a few milliseconds. This study allowed to evaluate and to validate the numerical hydrocode model by means of three test cases.

References

[1] Schmidt E M. Measurement of sabot discard and analysis of associated launch disturbances, Technical Report ARBRL-TR-02157, April 1979.

[2] Hruschka R, and Sauerwein B. Influence of molecular vibrational energy accommodation modeling on cone surface heat FLUX at Mach 10, *Journal of Energy and Power Engineering* 10, pp 660-666, 2016

[3] Schmidt E M. Wind tunnel measurements of sabot discard aerodynamics, Technical Report ARBRL-TR-02246, July 1980.

[4] Reck B, Sturtzer M O, Allen R and Eckenfels D. Ballistic pendulum for blast wave impulse measurement – analysis and optimization. *20th International Symposium on Military Aspects of Blast and Shock MABS20*, Oslo, Norway, Sept. 1- 5, 2008.

[5] Autodyn Theory Manual, Rev. 4.3. Century Dynamics, 2003

[6] Zalesak S T. Fully multidimensional flux-corrected transport algorithms for fluids. *Journal of Computational Physics*, Vol. 31, 335-362, 1979.

[7] .AUTODYN User Manual Version 12.1, Ansy Inc., November 2009

[8] Feszty, D., Badcock, K. J., and Richards, B. E.: "Driving mechanisms of high-speed unsteady spiked body flows, Part 1: Pulsation Mode" AIAA Journal, V. 42 No. 1, pp. 95-106 (2004)

Copyright Statement